



Delft University of Technology

Quantification of Tidal Asymmetry and Its Nonstationary Variations

Guo, Leicheng; Wang, Zhengbing ; Townend, Ian; He, Qing

DOI

[10.1029/2018JC014372](https://doi.org/10.1029/2018JC014372)

Publication date

2019

Document Version

Submitted manuscript

Published in

Journal Of Geophysical Research-Oceans

Citation (APA)

Guo, L., Wang, Z., Townend, I., & He, Q. (2019). Quantification of Tidal Asymmetry and Its Nonstationary Variations. *Journal Of Geophysical Research-Oceans*, 124(1), 773-787. <https://doi.org/10.1029/2018JC014372>

Important note

To cite this publication, please use the final published version (if applicable). Please check the document version above.

Copyright

Other than for strictly personal use, it is not permitted to download, forward or distribute the text or part of it, without the consent of the author(s) and/or copyright holder(s), unless the work is under an open content license such as Creative Commons.

Takedown policy

Please contact us and provide details if you believe this document breaches copyrights. We will remove access to the work immediately and investigate your claim.

1 **Quantification of tidal asymmetry and its non-stationary variations**

2

3 Leicheng Guo ^{a,*}, Zheng Bing Wang ^{a,b,c}, Ian Townend ^{a,d}, Qing He ^a

4

5 ^a State Key Lab of Estuarine and Coastal Research, East China Normal University,
6 Shanghai 200062, China

7 ^b Department of Hydraulic Engineering, Faculty of Civil Engineering and Geosciences,
8 Delft University of Technology, Delft 2600GA, the Netherlands

9 ^c Marine and Coastal Systems Department, Deltares, Delft 2629 HV, the Netherlands

10 ^d School of Ocean and Earth Sciences, University of Southampton, Southampton, UK

11

12 * Corresponding author, E-mail: lcguo@sklec.ecnu.edu.cn

13

14 **Key points**

15 1. Both harmonic and statistical methods are effective in indicating tidal asymmetry.

16 2. Statistical methods are applicable in quantifying non-stationary variations.

17 3. We find non-linear effects of river discharge on tidal asymmetry in long estuaries.

18

19

20 **Abstract**

21 Tidal wave deformation and tidal asymmetry widely occur in tidal estuaries and
22 lagoons. Tidal asymmetry has been intensively studied because of its controlling role
23 on residual sediment transport and large-scale morphological evolution. There are
24 several methods available to characterize tidal asymmetry prompting the need for an
25 overview of their applicability and shortcomings. In this work we provide a brief
26 review and evaluation of two methods, namely the harmonic method and the
27 statistical method. The latter comprises several statistical measures that estimate the
28 probability density function and various forms of skewness. We find that both the
29 harmonic and statistical methods are effective and have complementary advantages.
30 The harmonic method is applicable to predominantly semi-diurnal or diurnal regimes,
31 while the statistical methods can be used in mixed tidal regimes. Assisted by harmonic
32 data, a modified skewness measure can isolate the contribution of different tidal
33 interactions on net tidal asymmetry and also reveal its subtidal variations. The
34 application of the skewness measure to non-stationary river tides reveals stronger tidal
35 asymmetry during spring tides than neap tides, and the non-linear effects of river
36 discharges on tidal asymmetry in the upper and lower regions of long estuaries.

37

38 **Key words:** Tidal asymmetry; Harmonic; Skewness; Residual sediment transport

39

40

41 **Plain Language Summary**

42 Astronomical tide is the primary forcing that drives water motion and subsequent
43 sediment transport and morphological changes in coastal and estuaries waters. Tidal
44 waves propagating from open oceans into tidal estuaries and lagoons often experience
45 changes in wave amplitude, speed, and shape, displaying tidal wave deformation and
46 associated tidal asymmetry that is featured by unequal rising and falling tidal periods.
47 This work first provides a brief review of the methods available for the quantification
48 of tidal asymmetry in varying tidal environments, and discusses their applicability
49 based on constructed data. The application of these two methods to measured
50 non-stationary tides in a long estuary, under significant time-varying river discharges,
51 reveals strongly non-linear and non-uniform features of tidal asymmetry. The findings
52 of this work have implications for the interpretation of high water levels in flood
53 management and large scale estuarine morphological evolution.

54

55

56 **1. Introduction**

57 Sediment transport is a focal point in coastal management, particularly in tidal
58 estuaries and lagoons where there is conflicting interest between coastal developments
59 and tidal wetland conservation under sea-level rise. Other than the controlling impacts
60 of sediment source availability, the dynamic processes leading to residual
61 (tide-averaged) sediment transport are of significant relevance in examining erosion
62 and deposition and consequent morphological changes (Dronkers, 1986). Tidal
63 asymmetry is recognized as one of the most important processes in creating residual
64 sediment transport and associated large-scale morphological changes in tidal
65 environments including estuaries, tidal inlets and lagoon systems, and coastal waters
66 (de Swart and Zimmerman, 2009). Tidal asymmetry in general refers to the
67 phenomenon of tidal wave deformation (Pugh, 1987; Friedrichs and Aubrey, 1988).
68 This leads to an unequal duration of the rise and fall of the height of the tide (vertical
69 tide) and consequently, offsets between the strength of the flood and ebb velocities
70 (horizontal tide). Moreover, examination of tidal wave deformation and tidal
71 asymmetry also deepens our understandings of tidal dynamics in shallow coastal
72 waters and has implication as regards coastal flooding and management (Godin, 1985,
73 1999; Guo et al., 2015). Overall, tidal asymmetry has been well-examined regarding
74 its behavior and variability (Dronkers, 1986; Friedrichs and Aubrey, 1988; Wang et al.
75 1999) and its controlling effects on residual sediment transport and large-scale
76 morphodynamics (Postma, 1961; Guo et al., 2016a, b; Gatto et al., 2017).

77 In this work we discuss three types of tidal asymmetry: (1) unequal rising and
78 falling tidal durations of vertical tides, called *tidal duration asymmetry*, (2) uneven
79 peak ebb and flood velocities, called *peak current asymmetry*, and (3) unequal high
80 water and low water slack durations in tidal currents, called *slack water asymmetry*
81 (Dronkers, 1986; Gong et al., 2016; Guo et al., 2018). A shorter rising tide than falling
82 tide, stronger peak flood currents than ebb currents, or a longer high water slack than
83 low water slack result in flood dominance. Conversely a shorter falling tide, stronger
84 ebb currents, or longer low water slack promote ebb dominance. Flood dominance
85 will cause flood-directed residual sediment transport, sediment import and tidal basin

86 infilling, while ebb dominance will cause seaward sediment flushing, sediment export
87 and tidal estuary emptying.

88 Tidal duration asymmetry has been more widely examined compared to peak
89 current asymmetry, and slack water asymmetry because tidal water level data are
90 readily more available than tidal currents. Tidal duration asymmetry and peak current
91 asymmetry are coherently connected, such that a shorter rising tide will lead to
92 stronger flood currents in the absence of significant river discharges. In addition,
93 non-tidal forcing such as river discharge and storm surges etc. can profoundly
94 modulate tidal propagation and deformation, thus altering tidal asymmetry as well.
95 Storm surges affect tidal waves given their comparable space and time scales in
96 shallow waters (LeBlond, 1991). River discharge is usually non-stationary and can
97 raise mean water level (Cai et al., 2016), reduce tidal amplitudes, retard tidal phases
98 (Godin, 1985, 1991), and enhances wave deformations (Guo et al., 2015) inside tidal
99 estuaries. The duration of rising tides become shorter and falling tides become longer
100 under a significant river discharge, suggesting enhanced tidal wave deformation.
101 Moreover, non-tidal forcing and/or hypsometric effects of inter-tidal flats may cause
102 modification of tidal currents such that tidal duration asymmetry and peak current
103 asymmetry may become inconsistent, e.g., shorter rising tide coexists with stronger
104 ebb currents in tidal estuaries with a significant river discharge (Friedrichs and Aubrey,
105 1988; Guo et al., 2014). These variations ask for more specific examinations of tidal
106 asymmetry by different quantification methods.

107 A number of studies have examined the nature and variability of tidal asymmetry
108 in varying tidal environments (Aubrey and Speer, 1985; Speer and Aubrey, 1985;
109 Friedrichs and Aubrey, 1988; Wang et al., 1999, 2002; Nidzieko, 2010; Song et al.,
110 2011; Guo et al., 2018). Different methods are used to characterize and quantify tidal
111 asymmetry, but so far the applicability, advantages and shortcomings of these
112 methods have not been addressed. In this work we provide a review and evaluation of
113 two methods available as hydraulic measures of tidal asymmetry, namely: (1)
114 harmonic method, which is based on the phase differences and amplitude ratios of the
115 interacting tidal constituents, and (2) a set of statistical measures that estimate

116 probability density function (PDF) and various forms of skewness using tidal heights
117 or tidal currents. Other than the hydraulic measures, there are morphological metrics
118 which are used to characterize tidal asymmetry and residual sediment transport, e.g.,
119 the proxy using tidal amplitude to water depth ratio and inter-tidal storage volume to
120 channel volume ratio (Friedrichs and Aubrey, 1988), and an indicator based on
121 relative change rates of high water and low water surface area (Dronkers, 1986).
122 These morphological metrics have recently been reviewed by Zhou et al. (2018) and
123 link closely to the hydraulic measure examined in this work.

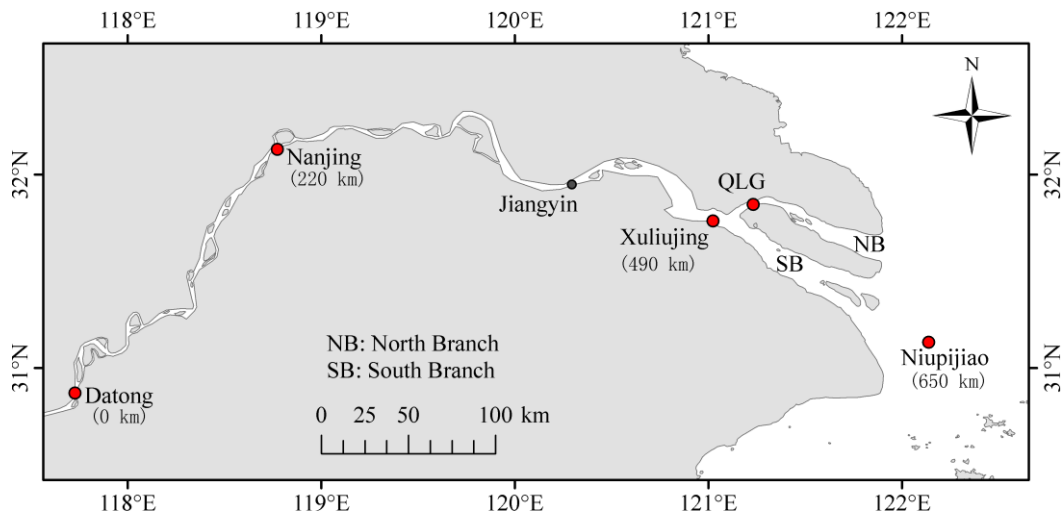
124

125 **2. Data used**

126 We apply the methods to two types of data to provide a comprehensive evaluation
127 of their applicability in varying environments. The first data are reconstructed tidal
128 signals based on the harmonic constants of user-selected constituents, e.g., the
129 reconstructed signals based on M_2+M_4 or $M_2+O_1+K_1$ constituents with different
130 amplitudes and phases. These datasets are used to check the effectiveness of different
131 methods when the nature of tidal asymmetry is straightforward to detected from the
132 signals. Application and discussion of these data follows the descriptions of the
133 methods in section 3.

134 The second type of data are actual tidal height measurements in the Changjiang
135 River estuary in China that is used to demonstrate the advantages and shortcoming of
136 the methods (Figure 1). The Changjiang River estuary is a meso-tidal coastal plain
137 estuary physically forced by mixed tides with tidal ranges up to 5 m and a river
138 discharges seasonally varying in the range of 10,000-60,000 m^3/s at Datong (the tidal
139 wave limit) (Guo et al., 2015). Tidal wave propagation in the Changjiang River
140 estuary is modulated by basin geometry, shallow water effects, and highly varying
141 river discharges, thus exhibiting strong tidal wave deformation and non-stationary
142 behaviors and associated spatial variability. For instance, strong tidal wave
143 amplification and tidal bores take place in the landward portion of the North Branch,
144 e.g., at Qinglonggang (QLG, because of high convergence and the limited influence of
145 river discharge; Figure 1), displaying a different behavior to the South Branch (see

146 section 4.1). Moreover, we also collect one-year tidal height data (hourly interval) at
 147 80 gauges along the US coasts from websites of NOAA (<https://co-ops.nos.noaa.gov>)
 148 (see Figure S1). Only the gauges along the open coasts are selected (those inside
 149 estuaries and lagoons are omitted to avoid river influences). Furthermore, we also
 150 include tidal current data which are from a numerical model of a short tidal estuary,
 151 the Newport Bay in southern California (see section 3.2). More descriptions of the
 152 tidal data in the Changjiang River estuary and in Newport Bay can be found in Guo et
 153 al. (2015) and Guo et al. (2018), respectively, thus are not repeated here. Tidal
 154 harmonic analysis is then performed to the tidal height and tidal current data by using
 155 the T_Tide function (Pawlowicz et al., 2002), which outputs tidal harmonics
 156 (amplitudes and phases) for quantification of the tidal asymmetry.



157
 158 **Figure 1.** Sketch of the Changjiang River estuary and tidal gauges. The numbers in
 159 the brackets indicate the seaward distance to Datong, the tidal wave limit in the dry
 160 season. Niupijiao represents the river mouth, and Xuliujing and Nanjing represents the
 161 lower and upper estuary, respectively, with the division roughly at Jiangyin (Guo et al.,
 162 2015). QLG is the abbreviation of Qinglonggang. The smaller dots indicate other tidal
 163 gauges though their data are not included in this work.

164

165 3. Methods review

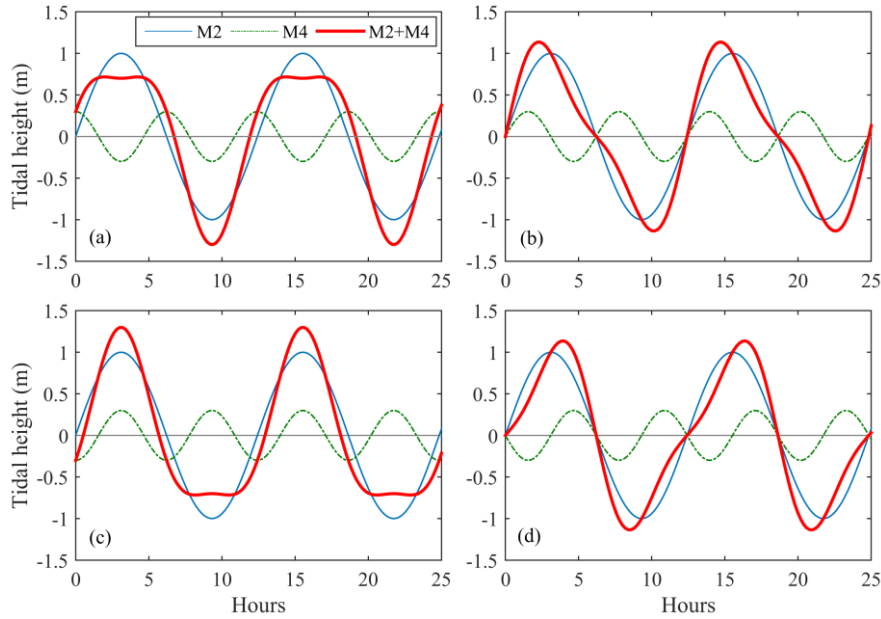
166 In this section we present two types of method, namely the harmonic method and
 167 the statistical method. The harmonic method has been widely used in previous studies,

168 and the occurrence of tidal asymmetry is evaluated based on the phase differences of
169 the tidal constituents (resolved by harmonic analysis of tidal water levels or tidal
170 currents) that interact and create tidal wave deformation (section 3.1). The statistical
171 methods have several forms, including calculating the probability distribution
172 function of tidal heights and (rising and falling) tidal durations (section 3.2), and
173 evaluating the skewness of the time derivative of tidal water levels or the transformed
174 skewness of tidal water levels (section 3.3). These statistical methods do not rely on
175 harmonic analysis but, instead, examine the statistical properties of tidal waves to
176 infer wave deformation and consequent tidal asymmetry.

177 **3.1 Harmonic method**

178 The harmonic method used to characterize tidal asymmetry is based on the tidal
179 harmonics (amplitudes and phases of tidal constituents) resolved from actual tidal data.
180 Two indicators are included, i.e., the phase differences and amplitude ratios between
181 two or more tidal constituents that interact and generate tidal asymmetry. As indicated
182 in Song et al. (2013), the interacting tidal constituents satisfying a frequency
183 relationship such as $2\omega_1=\omega_2$, $3\omega_1=\omega_2$, $\omega_1+\omega_2=\omega_3$ (ω is frequency, the subscript
184 indicates different tidal constituents) can generate tidal asymmetry. Hence the phase
185 differences such as $2\theta_1-\theta_2$, $3\theta_1-\theta_2$, and $\theta_1+\theta_2-\theta_3$ (θ is phase) are used to indicate the
186 nature of tidal asymmetry. For instance, the M_2 - M_4 interactions ($2\omega_{M_2}=\omega_{M_4}$) are
187 widely recognized as the dominant cause of tidal wave deformation and associated
188 tidal asymmetry (Speer and Aubrey, 1985; Friedrichs and Aubrey, 1988). Therefore a
189 phase difference of $2\theta_{M_2}-\theta_{M_4}$ in the range of $0\sim 180^\circ$ leads to a shorter rising tide than
190 falling tide thus flood dominance (Figure 2b), while a phase difference in the range of
191 $180\sim 360^\circ$ leads to a shorter falling tide and ebb dominance (Figure 2d). A $2\theta_{M_2}-\theta_{M_4}$
192 phase difference of exactly 0 or 180° will lead to equal rising and falling tides thus no
193 tidal asymmetry though the wave shape is statistically skewed (Figures 2a and 2c).
194 Under the same phase difference, the A_{M_4}/A_{M_2} amplitude ratio (A is tidal amplitude) is
195 used to indicate the magnitude of the tidal asymmetry. A larger amplitude ratio implies
196 stronger tidal wave deformation and tidal asymmetry. Successful applications of the
197 harmonic method to predominantly semi-diurnal regimes, e.g., US Atlantic coasts

198 (Friedrichs and Aubrey, 1988), Dutch coasts (Wang et al., 1999), and idealized tidal
 199 basins driven by M_2 tide only (Guo et al., 2014), have confirmed its effectiveness.



200
 201 **Figure 2.** Tidal heights by M_2 , M_4 and M_2+M_4 tides with a phase difference $2\theta_{M_2}-\theta_{M_4}$
 202 of (a) 0° , (b) 90° , (c) 180° , and (d) 270° . The A_{M_4}/A_{M_2} amplitude ratio is 0.3.

203
 204 Similarly, the dual tidal interactions such as M_2-M_6 ($3\omega_{M_2}=\omega_{M_6}$) and K_1-K_2
 205 ($2\omega_{K_1}=\omega_{K_2}$) can generate tidal asymmetry, and they can be quantified by phase
 206 differences such as $3\theta_{M_2}-\theta_{M_6}$ (Blanton et al., 2002) and $2\theta_{K_1}-\theta_{K_2}$ (Jewell et al., 2012),
 207 respectively. Moreover, triad tidal interactions such as $M_2-M_4-M_6$ ($\omega_{M_2}+\omega_{M_4}=\omega_{M_6}$),
 208 $M_2-S_2-MS_4$, $M_2-N_2-MN_4$, $M_2-O_1-K_1$, and $S_2-K_1-P_1$ have been shown to generate
 209 measurable tidal asymmetry in tidal estuaries, and accordingly the tidal asymmetry
 210 can be quantified by phases differences of $\theta_{M_2}+\theta_{M_4}-\theta_{M_6}$, $\theta_{M_2}+\theta_{S_2}-\theta_{MS_4}$, $\theta_{M_2}+\theta_{N_2}-\theta_{MN_4}$,
 211 $\theta_{O_1}+\theta_{K_1}-\theta_{M_2}$, and $\theta_{K_1}+\theta_{P_1}-\theta_{S_2}$, respectively (van de Kreeke and Robaczewska, 1993;
 212 Hoitink et al., 2003; Song et al., 2011; Guo et al., 2016a). A phase difference in the
 213 range of $0\sim 180^\circ$ will cause a shorter rising tide than falling tide and flood dominance,
 214 similar in the $2\theta_{M_2}-\theta_{M_4}$ case.

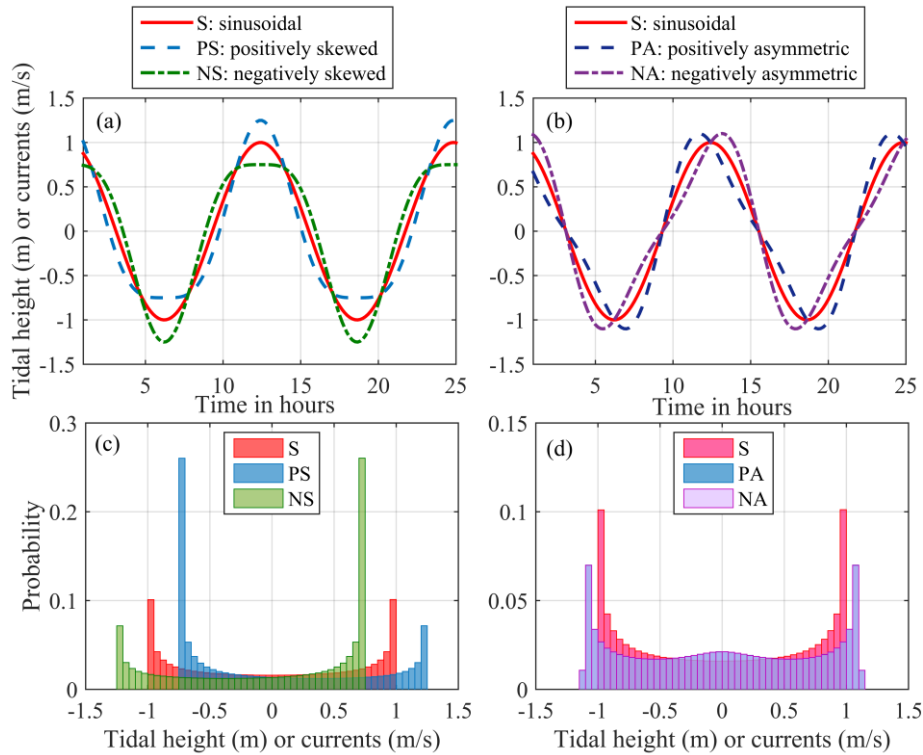
215 The harmonic method can be used to indicate peak current asymmetry in a similar
 216 way as tidal duration asymmetry based on the harmonics of resolved tidal currents. In
 217 short tidal basins with limited inter-tidal flats and insignificant river discharge where
 218 standing waves form, vertical tides and horizontal tides are in quadrature (Nidzieko,

219 2010). Therefore, a phase difference of tidal currents, e.g., $2\Phi_{M2}-\Phi_{M4}$ or $\Phi_{O1}+\Phi_1-\Phi_{M2}$
220 (Φ is phase of horizontal tides), in the range of $90\sim 270^\circ$ indicates ebb dominance and
221 that between -90° and 90° indicates flood dominance (Friedrichs and Aubrey, 1988;
222 Guo et al., 2014, 2016a). For instance, the phase differences of $\theta_{O1}+\theta_{K1}-\theta_{M2}$ and
223 $\Phi_{O1}+\Phi_1-\Phi_{M2}$ are 253° and 181° , respectively, in Newport Bay, both indicating ebb
224 dominance (Guo et al., 2018). It is understandable because a shorter falling tide than
225 rising tide needs larger ebb currents to convey the same tidal prism, thus ebb
226 dominance takes place.

227

228 **3.2 Statistical method**, measure I- probability density function

229 In addition to the harmonic method, tidal asymmetry has been characterized by
230 statistical measures. One approach is to use the PDF of the time series of tidal heights
231 (referenced to mean water level); referred to as the Tidal Height PDF, or TH-PDF. We
232 see that a symmetric sinusoidal tidal signal has a bimodal distribution for the TH-PDF.
233 Deviation from this bimodal distribution suggests wave shape deformation although
234 not necessarily tidal asymmetry (Ranasinghe and Pattiaratchi, 2000). For instance, the
235 TH-PDFs of the constructed tidal signals (reconstructed based on M_2 and M_4
236 constituents as shown in Figure 2) with or without tidal asymmetry are similarly
237 symmetric, thus we can not tell which one is flood or ebb dominant (Figure 3). To
238 overcome that, Castanedo et al. (2007) reported a wave-by-wave method to
239 characterize tidal statistics by estimating the PDFs of four variables, i.e., the time
240 series of wave crest (a) and trough (b) amplitudes, mean level (m), and standard
241 deviation (s) of the tidal height. A sinusoidal wave without tidal asymmetry will have
242 $a=b=A$, $m=0$, and $s=\sqrt{2}A/2$. Based on a long time series of tidal height data, a
243 scatter plot of the four variables against tidal height will exhibit deviations from their
244 values for symmetric sinusoidal waves, thus possibly indicating tidal asymmetry.
245 However, this wave-by-wave method only indicates the occurrence of tidal
246 asymmetry but not its nature (flood or ebb dominance).



247

248 **Figure 3.** (a) Skewed and (b) asymmetric tidal wave or tidal current curves, and (c, d)
 249 their corresponding PDFs. The positively and negatively asymmetric curves in pane
 250 (b) have the same PDF thus they are overlapped in panel (d). The flood currents are
 251 positive and ebb currents are negative in panel (a) and (b).

252

253 Another approach is based on the PDF measure of the time series of rising
 254 (indicated with a positive sign) and falling (indicated with a negative sign) tidal
 255 durations; referred to as the Tidal Duration PDF, or TD-PDF. The rising and falling
 256 tidal durations are directly derived from the tidal water level data. Statistical
 257 indicators of the TD-PDF are then used to quantify tidal duration asymmetry, e.g., the
 258 skewness indicator (see section 3.3). In a simplified form, an equal percentage of
 259 rising and falling tidal durations indicates no tidal asymmetry, whilst flood dominance
 260 occurs when the average rising tidal duration is <50% of the total period, and the
 261 converse is true for ebb dominance (Lincoln and Fitzgerald, 1988; Jewell et al., 2012).
 262 Such a definition is consistent with the concept of tidal duration asymmetry, and it is
 263 theoretically applicable to all tidal regimes. Application of the TD-PDF to the
 264 constructed tidal signals (see Figure 2) suggests a percentage of rising tidal durations

265 of 36% and 64% for the composite M_2+M_4 tides in Figure 2b and Figure 2d,
266 respectively, suggesting flood dominance and ebb dominance that agrees with the
267 harmonic method. Note that hourly tidal water level data are not enough to provide an
268 accurate estimation of the falling and rising tidal durations, thus long-time series of
269 data with a high time resolution are needed to accomplish significant differences
270 between falling and rising tidal durations and to get rid of short-term periodic
271 variability when the tidal signals are complex (see section 4.1).

272 The PDF measure also applies to the characterization of peak current asymmetry
273 by examining the PDF of tidal currents; referred to here as the Tidal Current PDF, or
274 TC-PDF. Being similar to the TD-PDF, a larger percentage (>50%) of flood currents
275 than ebb currents, i.e., a higher probability of the occurrence of flood currents,
276 indicates flood dominance, when assuming flood currents are positive and ebb
277 currents are negative (Ranasinghe and Pattiaratchi, 2000). Moreover, the TC-PDF is
278 better estimated by using u^3 instead of u (u is tidal current) to account for the
279 non-linear relationship between sediment transport and velocity, i.e., an exponentially
280 higher sediment transport capacity for larger current velocities (see Figure S2). A
281 larger percentage of the cubed flood currents than cubed ebb currents indicate flood
282 dominance. The TC-PDF is similar to the skewness measure that considers a cubic
283 numerator of currents (see Eq. 1 in section 3.3).

284

285 **3.3 Statistical method, measure II - skewness**

286 *Statistical skewness*

287 Skewness is a statistical measure of the asymmetry present in the PDF of an input
288 signal compared to a normal distribution. The skewness measure characterizes the
289 degree of asymmetry about the horizontal axis (up-and-down asymmetry) and the
290 asymmetry measure represents the degree of asymmetry about the vertical axis
291 (front-and-back asymmetry) of a PDF. The skewness indicator is calculated as
292 follows:

$$Sk(x) = \frac{\frac{1}{N-1} \sum_{t=1}^N (\eta_t - \bar{\eta})^3}{\left[\frac{1}{N-1} \sum_{t=1}^N (\eta_t - \bar{\eta})^2 \right]^{3/2}} \quad (\text{Eq. 1})$$

where Sk is the skewness indicator, x_t is the time series of the input signal, $\bar{\eta}$ is the mean value, and N is the length of equidistant time series data. The skewness method has been used in a wide variety of geophysical fields, such as for the characterization of turbulence non-linearity in fluid mechanics and acoustic wave transformation etc. (Shepherd et al., 2011; Reichman et al., 2016). A positive skewness of an input signal indicates a longer and/or flatter tail on the right side of its PDF (median value < mean value), and conversely a negative skewness indicates a longer and/or flatter tail on the left side (median value > mean value).

When applying Eq. (1) to tidal water levels, we see that the skewness indicators are non-zero for both the positively and negatively skewed signals in Figure 3a (i.e., skewed TH-PDF), whereas actually both signals have equal rising and falling tidal durations (i.e., no tidal asymmetry). Similarly, the skewness indicators are zero for both the positively and negatively asymmetric signals in Figure 3b (i.e., non-skewed TH-PDF), whereas the two signals actually have unequal rising and falling durations (i.e., with tidal asymmetry). It thus implies that using the tidal water levels as input signals in Eq. (1) can not indicate tidal asymmetry, and some modification of this method are outlined in the following sections.

311

312 ***Transformed skewness***

One solution is to use an asymmetry proxy, a transformed skewness measure. It is a skewness measure of the imaginary part of a Hilbert-transformed input signal. It reads as:

$$As = Sk\{imag[H(\eta)]\} \quad (\text{Eq. 2})$$

where As is the transformed skewness measure, $H(\cdot)$ indicates the Hilbert transform, and $imag(\cdot)$ indicates the imaginary part (the real part of the output of a Hilbert transform is the input signal itself). The transformed skewness measure has been used

320 in characterizing wave-induced current asymmetry under short wave impacts
321 (Ruessink et al., 2009). For a time-series of tidal water levels, the imaginary part of a
322 Hilbert-transformed tidal height leads to positive and negative outputs for falling and
323 rising tides, respectively (see Figure S3). Therefore, a positive value of the
324 transformed skewness measure suggests longer rising tidal durations than falling tide
325 durations on average (i.e., ebb dominance), and a negative value indicates longer
326 falling tidal durations (i.e., flood dominance) (Bruder et al., 2014). To further validate
327 the general effectiveness of the transformed skewness, we apply it to the constructed
328 signals in Figure 3 and find that the transformed skewness is consistently zero for the
329 sinusoidal signal (S), and the positively (PS) and negatively (NS) skewed signals in
330 Figure 3a, thus implying no tidal asymmetry. The transformed skewness is -0.48 and
331 0.48 for the positively (PA) and negatively (NA) asymmetric signals in Figure 3b,
332 suggesting longer falling and rising tidal durations, respectively. The evaluation by
333 the transformed skewness measure is therefore consistent with the harmonic method,
334 demonstrating its effectiveness as a suitable measure of tidal asymmetry.

335

336 *Derivative skewness*

337 Another option of is to use the time derivatives of tidal height as the input signal
338 in Eq. (1) instead of tidal height itself (Nidziedo, 2010), called derivative skewness, as
339 follows:

$$340 \quad Sk_{TDA} = Sk(d\eta/dt) \quad (\text{Eq. 3})$$

341 where TDA stands for tidal duration asymmetry. The time derivative ($d\eta/dt$)
342 transforms rising and falling tidal water levels into positive and negative gradients
343 (see Figure S3), thus enabling tidal duration asymmetry estimation in a similar way to
344 the Hilbert transform in Eq. 2. A positive derivative skewness indicates a shorter
345 rising tide than falling tide and flood dominance, while a negative derivative skewness
346 demonstrates a shorter falling tide and ebb dominance. Applying the derivative
347 skewness measure to the constructed signals will give zero value for signals S, PS and
348 NS in Figure 3a, but 0.76 and -0.76 for signals PA and NA, respectively, in Figure 3b,

349 implying its applicability. Note that the transformed and derivative skewness
350 measures have opposite sign for the same tidal asymmetry. The derivative skewness
351 method was further extended and used to isolate the contribution of tidal interactions
352 like M_2 - M_4 , M_2 - O_1 - K_1 , and S_2 - K_1 - P_1 etc. on the total tidal asymmetry (Song et al.,
353 2011), and to uncover fortnightly variations of tidal duration asymmetry when
354 applying Eq. (3) using a moving window (e.g., 3 days) (Guo et al., 2016b).

355

356 When applying the transformed skewness (Eq. 2) and derivative skewness (Eq. 3)
357 measures in their present form, we find that the cubic numerator in the skewness
358 indicator (in Eq. 1) will amplify the rising and falling rates of tidal height and this
359 nonlinear amplification may cause misleading results. Preliminary tests of the
360 derivative skewness method on artificially generated signals (with fixed falling and
361 rising tidal duration but different rising and falling limbs) suggested that the
362 derivative skewness varies in a considerable range, e.g., -0.1~1.2, and can be even
363 negative when the rising tide is actually shorter than falling tide (see Figure S4). A
364 similar discrepancy also occurs for the transformed skewness given by Eq. 2 (see
365 Figure S4). The discrepancies occur because the cubic numerator in Eq. 1 will
366 significantly increase the statistical importance of large derivatives (e.g., large tidal
367 height rising and falling rates). With respect to the shape of a PDF, the statistical
368 skewness does not distinguish the impacts of a long or a flat tail; therefore zero
369 skewness may indicate a symmetric PDF, or an asymmetric PDF with a long tail and a
370 flat tail on either side when the asymmetry evens out. To overcome this, Guo et al.
371 (2018) suggested an improvement by employing the derivative skewness to the time
372 series of high water (HW) and low water (LW), thus the nonlinear variations in the
373 rising and falling limbs of the tidal water level curves are removed and only the
374 duration differences between HW-LW or LW-HW will affect the skewness measure.
375 The calculation then reads as follow:

$$376 \quad Sk_{TDA} = Sk(d\eta_{HW-LW}/dt) \quad (\text{Eq. 4})$$

377 where η_{HW-LW} indicates the filtered time series signals with HW and LW only (with

378 linear interpolation between HW and LW to obtain equidistance data if necessary).
 379 The same HW-LW series of data can be also used as input to the transformed
 380 skewness measure. Preliminary application of the filtered derivative skewness has
 381 demonstrated its effectiveness to accurately indicate tidal duration asymmetry (Guo et
 382 al., 2018). When taking the derivative skewness of the filtered data as reference and
 383 applying both Eq. (3) and Eq. (4) to the tidal height data collected along the US coasts,
 384 we see that usage of the original signals will predominantly overestimate the
 385 magnitude of tidal asymmetry and the overestimation becomes larger for stronger
 386 tidal asymmetry (see Figure S5).

387

388 *Skewness measure applied to tidal currents*

389 The skewness measure is also applicable for quantification of peak current
 390 asymmetry and slack water asymmetry (Bruder et al., 2014; Gong et al., 2016; Guo et
 391 al., 2018). Skewed current curves (preponderance of large crests or troughs) have
 392 unequal peak ebb and flood currents, demonstrating the presence of peak current
 393 asymmetry but not slack water asymmetry (see Figure 3a). Similarly, asymmetric
 394 current curves have equal peak currents but uneven slack waters, thus indicating the
 395 presence of slack water asymmetry but not peak current asymmetry (see Figure 3b).
 396 The asymmetric current curves can be seen as acceleration-skewed, thus it is in line
 397 with the definition of slack water asymmetry. To use the skewness measure for
 398 quantification of peak current asymmetry (PCA), the input signal is tidal currents:

$$399 \quad Sk_{P_C \bar{A}} = Sk(u) \quad |u| > u_c \quad (\text{Eq. 5})$$

400 and for quantification of slack water asymmetry (SWA), the input signal is the
 401 acceleration of the currents:

$$402 \quad Sk_{S_W \bar{A}} = Sk(du/dt) \quad |u| < u_c \quad (\text{Eq. 6})$$

403 where u is a time series of tidal currents, and u_c is a velocity threshold to filter the
 404 tidal currents needed for transport of coarse sediments and for settling of fine
 405 sediments (Guo et al., 2018). Considering that sediment transport is a power function
 406 of velocity by an order of 3-5 (van Rijn, 1993), the skewness measure might be

407 expected to a good measure for quantifying the peak current asymmetry because the
408 cubic numerator in Eq. 1 emphasizes the sediment transport capacity of higher (both
409 ebb and flood) current velocities. Hence, it can be taken to be an effective
410 sediment-related tidal asymmetry indicator. When assuming flood currents are
411 positive, a positive PCA skewness indicates stronger flood currents and flood
412 dominance, and a positive SWA skewness indicates shorter low water slack and flood
413 dominance as well. When taking the signals in Figure 3 as tidal currents (and
414 assuming $u_c=0.2$ m/s), the PCA skewness of S, PS, and NS signals (see Figure 3a) is 0,
415 +0.49 (flood dominance), and -0.49 (ebb dominance), respectively, and the SWA
416 skewness of S, PA, and NA signals (see Figure 3b) is 0, +1.33 (flood dominance), and
417 -1.33 (ebb dominance), respectively. Gong et al. (2016) and Guo et al. (2018) had
418 applied the skewness method (Eq. 6) to indicate slack water asymmetry in estuaries.
419 These results demonstrate that the skewness measures (Eq. 5 and Eq. 6) can indicate
420 the peak current asymmetry and slack water asymmetry.

421

422 **4. Applications and evaluation**

423 **4.1 Application to actual data**

424 So far, we have shown that both the harmonic and statistical methods are effective
425 in indicating tidal asymmetry, when using constructed data. To further elaborate their
426 applicability and their advantages and shortcomings, we apply these methods to actual
427 tidal data obtained in the Changjiang River estuary. The tides in the Changjiang River
428 estuary are dynamically highly non-linear and non-stationary (Guo et al., 2015) hence
429 a single method is not able to characterize all tidal features and associated variations.
430 The harmonic method, the PDF measure and the filtered derivative skewness measure
431 are applied and evaluated. The transformed skewness measure works in a similar way
432 as the derivative skewness thus it is not discussed.

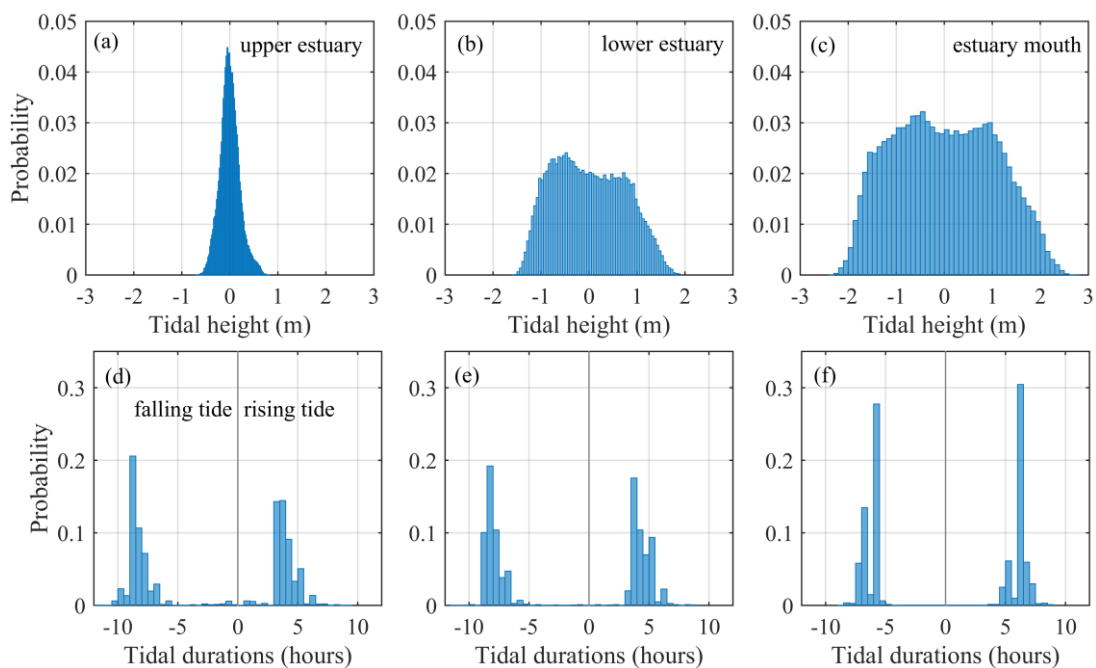
433 One year of tidal height data at three tidal gauges in the upper estuary, lower
434 estuary and estuary mouth are used to indicate along-river changes (see Figure 1).
435 Harmonic analysis suggests that the Changjiang River estuary has a mixed tidal
436 regime with an $(A_{O1}+A_{K1}+A_{P1})/(A_{M2}+A_{S2}+A_{N2})$ amplitude ratio of 0.24 at the mouth

437 (Guo et al., 2015). M_2 is the largest constituent, followed by S_2 , K_1 , O_1 , N_2 etc.
438 Overtide and compound tides such as M_4 and MS_4 are small outside the estuary but
439 become considerable inside the estuary (Guo et al., 2015). Past studies have shown
440 that any combination of more than two constituents (both principal and higher and
441 lower frequency harmonics) satisfying frequency relationships such as $2\omega_i=\omega_j$,
442 $\omega_i+\omega_j=\omega_k$, and $\omega_i+\omega_j+\omega_k=\omega_s$ etc. can create tidal asymmetry, e.g., M_2 - M_4 , M_2 - O_1 - K_1 ,
443 and M_2 - S_2 - N_2 - MSN_2 interactions (Le Provost, 1991; Song et al., 2011). Therefore,
444 tidal wave deformation and tidal asymmetry inside the Changjiang River estuary can
445 be induced by M_2 - M_4 , M_2 - O_1 - K_1 , M_2 - S_2 - MS_4 , M_2 - N_2 - MN_4 interactions etc (Guo et al.,
446 2015). The $2\theta_{M_2}-\theta_{M_4}$ phase difference is $\sim 70^\circ$ and varies little along the estuary,
447 suggesting flood dominance if considering M_2 - M_4 interactions only. The harmonic
448 analysis results show that the phase differences of $2\theta_{M_2}-\theta_{M_4}$, $\theta_{M_2}+\theta_{S_2}-\theta_{MS_4}$, and
449 $\theta_{M_2}+\theta_{N_2}-\theta_{MN_4}$ are nearly the same, and the $\theta_{O_1}+\theta_{K_1}-\theta_{M_2}$ phase difference varies
450 between 0 and 50° along the estuary (Guo et al., 2016a). It implies that all of these
451 tidal interactions will cause flood dominance. This result is in line with a shorter
452 rising tide than falling tide (see next paragraph). But it remains unknown which
453 interaction plays a bigger role in dominating the flood dominance. Note that the flood
454 dominance here refers to tidal water levels but not tidal currents (the ebb currents are
455 always stronger than flood currents because of significant river discharges). The
456 non-stationarity in the tidal signals induced by river discharge imposes a challenge to
457 resolve tidal harmonics precisely, particularly in the upper estuary where
458 non-stationary river influences are strong (Guo et al., 2015).

459 Strong tidal wave deformation and formation of tidal bores in the North Branch
460 of the Changjiang River estuary induce another difficulty for the harmonic method.
461 The tidal waves are much more deformed on spring tides than neap tides in the North
462 Branch, and tidal bores can be generated. The rising tides become much shorter while
463 the falling tides are prolonged under the occurrence of tidal bores (suggesting flood
464 dominance). These variations induce non-stationary behavior of tidal asymmetry.
465 Moreover, the high water may persist as long as 2.5 hours while the change from
466 falling to rising tide is sharp (see Figure S6). These peculiar features pose a challenge

467 for conventional harmonic analysis. With 38 tidal constituents resolved at QLG (see
 468 Figure 1), the harmonic methods show an identical phase difference of $2\theta_{M2}-\theta_{M4}$,
 469 $\theta_{M2}+\theta_{S2}-\theta_{MS4}$, $\theta_{M2}+\theta_{N2}-\theta_{MN4}$ of $\sim 82^\circ$ (suggesting flood dominance) but the phase
 470 difference of $\theta_{O1}+\theta_{K1}-\theta_{M2}$ is $\sim 350^\circ$ (suggesting ebb dominance). It is thus not possible
 471 to tell the nature of the net tidal asymmetry based on the harmonic method alone.
 472 Moreover, comparison of the reconstructed signals based on the resolved harmonic
 473 constants with the measured tidal heights shows that the harmonic analysis can not
 474 capture the flat high tide and sharp transition from falling to rising tide, leading to
 475 considerable discrepancies in the estimation of rising and falling tidal periods (see
 476 Figure S6).

477 Estimation of the average falling and rising tidal durations based on one-year tidal
 478 height data suggests that the mean falling tide duration is slightly longer (~ 0.03 hours)
 479 than rising tide at the estuary mouth and the duration inequality increases in the
 480 landward direction (e.g., falling tide is on average ~ 2.0 hours longer than rising tide in
 481 the upper estuary), reflecting a more distorted tidal wave in the inner estuary, owing to
 482 the combined impacts of friction, estuarine geometry, and river discharge. The PDFs
 483 of tidal heights show upstream tidal damping but not tidal asymmetry (Figures 4a-c),
 484 while the PDFs of falling and rising tidal durations confirm the observation that
 485 falling tides become increasingly longer in the landward direction (Figures 4d-f).



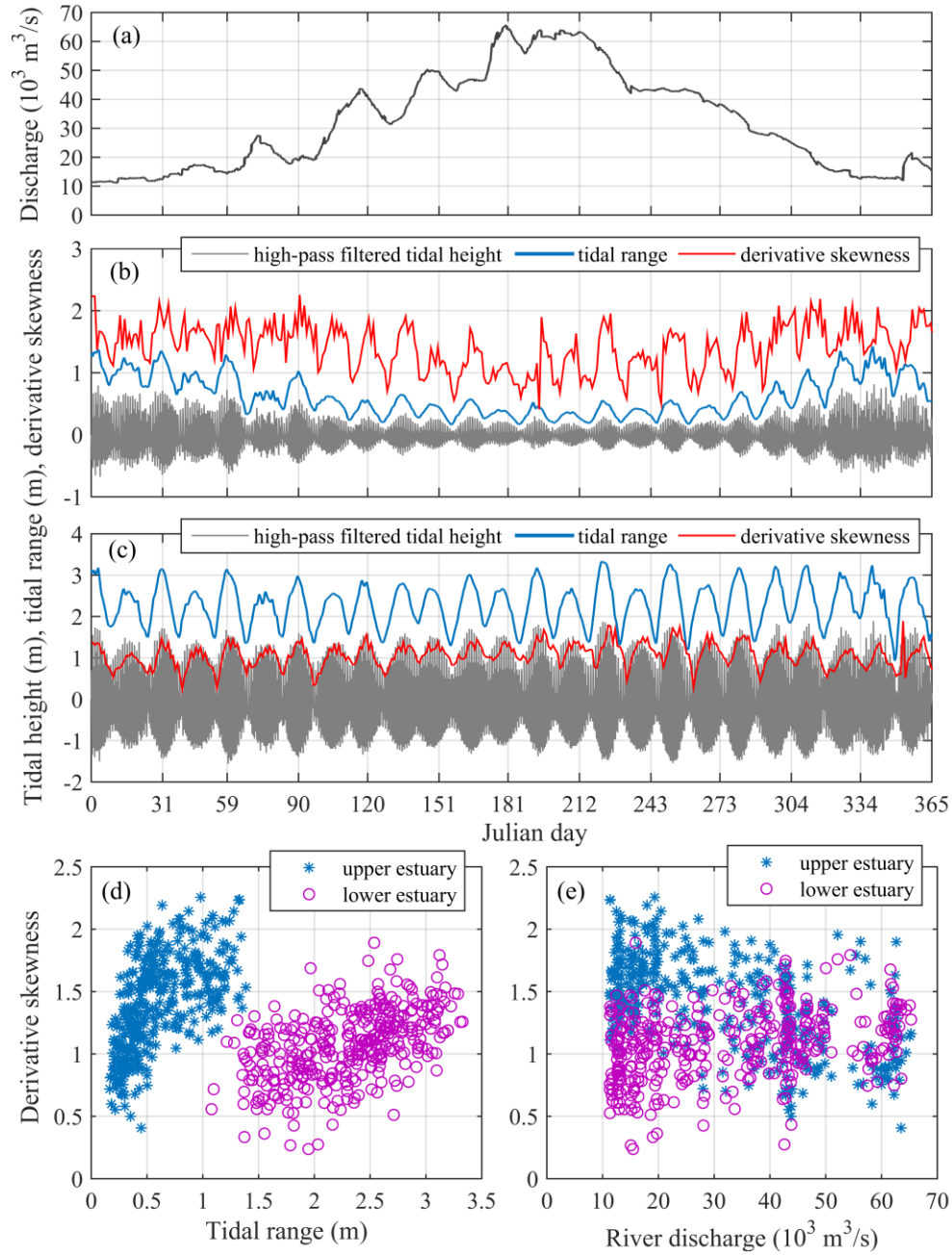
487 **Figure 4.** The TH-PDFs (a, b, c) and TD-PDFs (d, e, f) at stations in the upper estuary
488 (landward regions, Nanjing in Figure 1) (a, d), lower estuary (seaward regions,
489 Xuliujing) (b, e) and estuary mouth (Niupijiao) (c, f) based on 2-year data (2009-2010)
490 in the Changjiang River estuary. The tidal heights are referenced to local mean water
491 level. Rising tidal duration is positive and falling tidal duration is negative.

492
493 Application of the filtered derivative skewness method to the non-stationary river
494 tides in the Changjiang River estuary reveals strong subtidal variations of tidal ranges
495 and tidal duration asymmetry (Figures 5b and 5c) and associated non-uniform changes
496 in response to high and low river discharges (Figures 5d and 5e). The mean water
497 level and lower low tide are observed higher at spring tide than neap tide, in particular
498 in the upper estuary (LeBlond, 1991; Sassi and Hoitink, 2013; Guo et al., 2015). To
499 remove the influences of mean water levels, high-pass filtered data are used for the
500 derivative skewness measure. The derivative skewness for one-year data is 0.13, 1.37
501 and 2.32 at the mouth, in the lower and upper estuary, respectively, suggesting overall
502 shorter rising tides than falling tides throughout the estuary. Larger derivative
503 skewness in the upper estuary suggests enhanced tidal wave deformation in the
504 landward regions, particularly in the dry seasons when the river discharge is
505 significant but not too large (Figures 5b and 5c). At fortnightly time scales, the
506 derivative skewness is larger during spring tide than neap tide in both upper and lower
507 estuary, suggesting stronger wave deformation and tidal asymmetry during spring
508 tides (Figure 5d). At seasonal time scales, the derivative skewness decreases with
509 increasing river discharges in the upper estuary but increases in the lower estuary
510 (Figure 5e). It suggests that tidal duration asymmetry is stronger under high river
511 discharge in the lower estuary while it is smaller in the upper estuary. This result is
512 consistent with decreasing A_{D4}/A_{D2} ratios (the amplitude ratio of quarter-diurnal to
513 semi-diurnal species) in the upper estuary and increasing ratios in the lower estuary
514 with increasing river discharges in Guo et al. (2015). Analyses from a tidal energy
515 perspective also confirms the above finding. Work by Zhang et al. (2016) suggests
516 that the tidal asymmetry is one of the degrees-of-freedom used by the estuary to

517 maintain a state of minimum work, by adjusting tidal wave deformation and tidal
518 asymmetry along the estuary under varying river discharges.

519 The non-uniform behavior of tidal wave deformation between upper (landward)
520 and lower (seaward) regions of long tidal estuaries with significant river influence are
521 not unique to the Changjiang River estuary. Godin (1985, 1999) reported that a larger
522 river discharge will cause accelerated low water and retarded high water in the upper
523 St. Lawrence Estuary, whereas it will hasten the progress of high water and delay low
524 water in the lower estuary. Similar non-uniform changes also occur in the Amazon
525 Estuary (Gallo and Vinzon, 2005). Model results also reveal non-linear variations of
526 tidal asymmetry in response to increasing river discharges (Guo et al., 2016a). These
527 findings do not violate our intuitional understanding of the impacts of river discharge
528 in causing more tidal damping and wave distortion (throughout an estuary) because
529 both low and high river discharges will prolong falling tides and shorten rising tides
530 compared to the situation with zero river discharge.

531 The variations of the A_{D4}/A_{D2} amplitude ratios in response to increasing river
532 discharge in Guo et al. (2015) are consistent with the derivative skewness variations
533 in this work and it may imply that the M_2 - M_4 interaction is the dominant contribution
534 to net tidal duration asymmetry. Based on tidal harmonics and the decomposition
535 method suggested by Song et al. (2011), we estimate that the summed skewness of the
536 four major interactions, i.e., M_2 - M_4 , M_2 - O_1 - K_1 , M_2 - S_2 - MS_4 , and M_2 - N_2 - MN_4 , is 0.17
537 and 1.11, at the mouth and in the lower estuary, respectively. They are in good
538 agreement with the derivative skewness (0.13 and 1.37, respectively) obtained from
539 tidal height data. We see that the M_2 - M_4 interaction is indeed the major contribution to
540 the net tidal asymmetry, with a contribution >45% in the lower estuary, followed by
541 M_2 - S_2 - MS_4 (30%) and M_2 - N_2 - MN_4 (5%) interactions. The M_2 - O_1 - K_1 interaction is of
542 relatively minor importance (<1%) because of smaller O_1 and K_1 amplitudes
543 compared to M_2 and S_2 . Similarly, we quantify that the derivative skewness of tidal
544 height is 2.32 at QLG in the North Branch, and the contribution of M_2 - M_4 interaction
545 is 47% and that of M_2 - O_1 - K_1 interaction is -2% (negative value indicates a effect
546 causing ebb dominance).



547

548 **Figure 5.** (a) River discharge in calendar year 2010, (b) high-passed filtered tidal
 549 height, tidal ranges, and filtered derivative skewness in the (b) upper estuary (Nanjing,
 550 see Figure 1) and (c) lower estuary (Xuliujing), and (d) derivative skewness vs. tidal
 551 range, and (e) derivative skewness vs. river discharge in the Changjiang River estuary.

552

553 Quantification of peak current asymmetry under the influence of river discharges
 554 needs separate consideration. River discharge induces a seaward mean current (i.e.,
 555 $-u_o$, the negative sign indicates seaward) and enlarges ebb currents, causing overall

556 ebb dominance although the rising tides are shorter than the falling tides. Even though,
557 we find that the tide-related oscillatory currents (i.e., $\sum u_i \cos(\omega_i t + \theta_i)$, the subscript i
558 indicates the name of the tidal constituent), i.e., the high-pass filtered currents with the
559 mean current removed, are still stronger in the flood direction than the ebb direction.
560 For instance, with one-year of tidal current data at Xuliujing in the Changjiang River
561 estuary (Guo et al., 2015), we find that the high-pass filtered currents have a positive
562 PCA skewness of 0.03 based on Eq. 5 (assuming flood currents are positive),
563 suggesting stronger flood tidal currents and flood dominance. It is also validated by a
564 $2\Phi_{M2} - \Phi_{M4}$ phase difference of $\sim 25^\circ$ (in the range of $-90^\circ \sim 90^\circ$ thus indicating flood
565 dominance). Modeled tidal currents in a schematized estuary have also confirmed
566 flood dominance of tide-induced oscillatory currents although the ebb currents are
567 stronger than flood currents due to river discharge (Guo et al., 2014). Note that it is
568 the asymmetry in the total currents (i.e., $-u_o + \sum u_i \cos(\omega_i t + \theta_i)$) that controls the net
569 residual sediment transport, although the contribution of river and tide-related
570 asymmetry, and river-tide interaction can be decomposed (Guo et al., 2014, 2016a).

571

572 **4.2 Advantages and shortcomings of the methods**

573 The abovementioned applications and discussions suggest that both the harmonic
574 method and the statistical methods are effective in indicating and quantifying tidal
575 asymmetry although their applicability differs slightly (Table 1). The advantages of
576 the harmonic method include: (1) having a solid physical background and being
577 applicable to a large proportion of estuaries worldwide, where M_2 is the most
578 important principal constituent; (2) easy to use because of the availability of harmonic
579 constituent data for many locations, and (3) the impacts of non-tidal forcing are
580 accounted for by altered tidal amplitudes and phases. Its shortcoming lies in its
581 inability to characterize net tidal asymmetry in mixed tidal regimes where multiple
582 tidal interactions may either augment or cancel each other in creating tidal asymmetry,
583 as that has been identified by Jewell et al. (2012).

584

585 **Table 1.** A summary of the methods available for quantification of tidal asymmetry

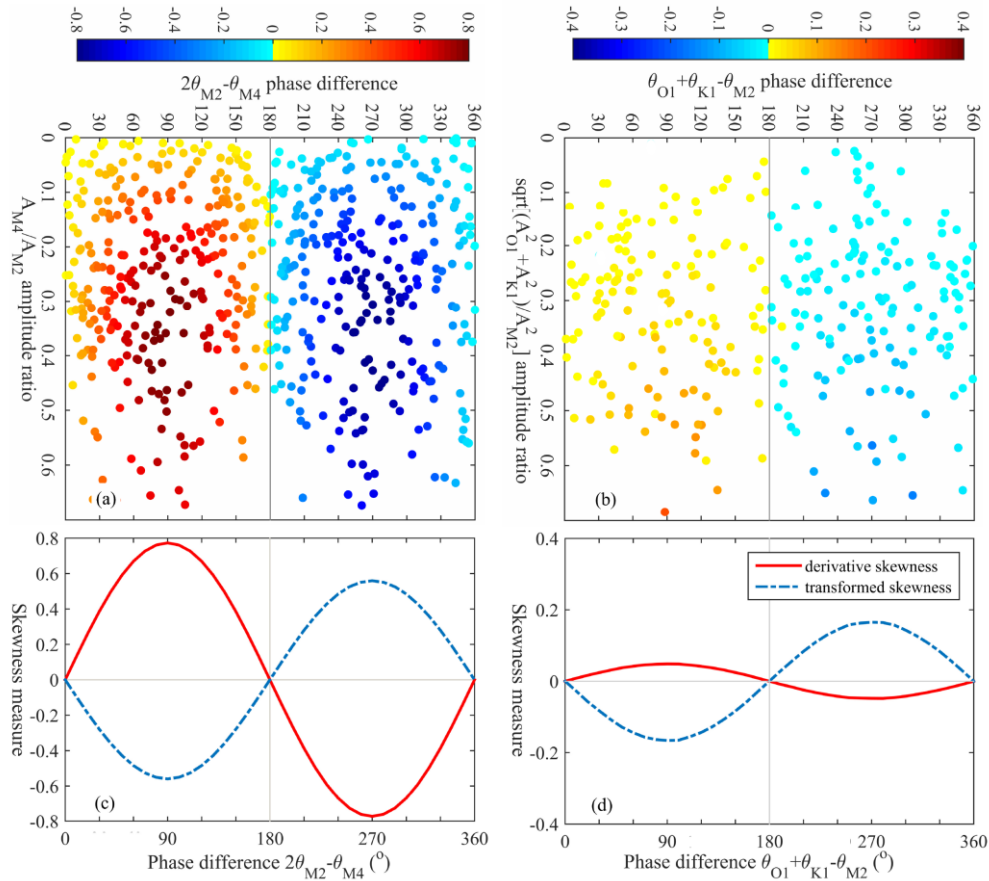
586 and their applicability and criterions in indicating flood or ebb dominance.

	Harmonic method	Statistical methods		
		PDF	Derivative Skewness	Transformed Skewness
Tidal Duration Asymmetry	<p>phase differences e.g., $2\theta_{M2}-\theta_{M4}$, $\theta_{O1}+\theta_{K1}-\theta_{M2}$</p> <p>phase differences in the range of $0\sim 180^\circ$ indicate flood dominance and that in the range of $180\sim 360^\circ$ indicates ebb dominance</p>	<p>TD-PDF of rising and falling durations, an average rising tidal duration $>$ or $<$ falling duration indicate ebb or flood dominance</p>	<p>skewness of time derivative of the time series of HW and LW, a derivative skewness $>$ or <0 indicates flood or ebb dominance, respectively</p>	<p>skewness of the imaginary part of Hilbert-transformed tidal water levels, a transformed skewness $>$ or <0 indicates ebb or flood dominance, respectively</p>
Peak Current Asymmetry	<p>phase differences e.g., $2\Phi_{M2}-\Phi_{M4}$, $\Phi_{O1}+\Phi_{K1}-\Phi_{M2}$,</p> <p>phase differences in the range of $90\sim 270^\circ$ indicate ebb dominance and that in the range of $-90\sim 90^\circ$ indicates flood dominance</p>	<p>TC-PDF of the cubed ebb and flood currents, a percentage of cubed flood currents $>$ or $<$ cubed ebb currents indicate flood or ebb dominance</p>	<p>skewness of tidal currents, a skewness $>$ or <0 indicates flood or ebb dominance, respectively (assuming flood currents are positive)</p>	not applicable
Slack Water Asymmetry	not applicable	applicable but has not been used	<p>skewness of tidal current accelerations, a skewness $>$ or <0 indicates flood or ebb dominance, respectively (assuming flood currents are positive)</p>	

587

588 On the other hand, we see that the derivative and transformed skewness measures
589 have advantages in terms of their ability to: (1) cope with complex tidal signals in
590 semi-diurnal, diurnal or mixed tidal regimes, (2) indicate net asymmetry caused by
591 multiple interactions and the separated contribution of individual interaction, (3)
592 reveal subtidal variations, and (4) quantify both tidal duration asymmetry and peak
593 current asymmetry. A weakness of the skewness method is the lack of strong physical
594 foundation. The sign of the derivative and transformed skewness measures indicates
595 the ebb or flood nature of tidal asymmetry, while its absolute value only indicates the
596 strength of tidal asymmetry in a relative manner. A physical understanding of the
597 connections between tidal wave deformation and the skewness proxy has yet to be
598 fully investigated.

599 Overall, we see that the harmonic, statistical PDF and skewness methods have
600 complementary advantages and are best used in combination. When plotting the
601 derivative skewness against the amplitude ratio (using the constructed signals
602 consisting of M_2+M_4 and $M_2+O_1+K_1$ constituents with different amplitude ratios and
603 phase differences) we clearly see that the derivative skewness is zero for phase
604 differences of 0 and 180° while it is maximal for phase differences of 90° and 270°
605 regarding both M_2-M_4 and $M_2-O_1-K_1$ interactions (Figure 6). The tidal asymmetry
606 induced by M_2-M_4 interaction tends to be strongest when the A_{M_4}/A_{M_2} ratio is 0.3-0.5
607 with a phase difference $2\theta_{M_2}-\theta_{M_4}$ of 90° or 270° (Figure 6a). We also see that the
608 derivative skewness is overall larger for the M_2-M_4 interaction (Figure 6a) than the
609 $M_2-O_1-K_1$ interaction (Figure 6b), suggesting possibly stronger effects of M_2-M_4
610 interaction in causing tidal asymmetry. These analyses suggest that the evaluations by
611 the harmonic method and the skewness measures can be somehow transformed.
612 Regarding their applicability, the harmonic method is preferred in predominantly
613 semi-diurnal or diurnal tidal regimes where single tidal interaction such as M_2-M_4 or
614 $M_2-O_1-K_1$ controls the tidal asymmetry. The statistical PDF and skewness methods are
615 the alternative options and have advantages in mixed tidal regime where multiple tidal
616 interactions occur.



617

618 **Figure 6.** Scatter plot of filtered derivative skewness of tidal duration asymmetry due
 619 to (a) M_2-M_4 and (b) $M_2-O_1-K_1$ interactions for ideally constructed signals with
 620 different phase differences and amplitude ratios, and (c, d) variations of derivative
 621 skewness and transformed skewness for an amplitude ratio of 0.3 but different phase
 622 differences. Positive derivative skewness and negative transformed skewness suggest
 623 flood dominance.

624

625 5. Conclusions

626 In this work we provide a brief review of two methods, i.e., the harmonic and
 627 statistical methods, available for quantification of tidal asymmetry and find that they
 628 have complementary advantages. By estimating phase differences and amplitude
 629 ratios, the harmonic method has a well-defined physical foundation and is applicable
 630 to semi-diurnal, or diurnal, tidal regimes. The statistics of the PDF of rising and
 631 falling tidal periods can be used to indicate tidal duration asymmetry and that of
 632 cubed tidal currents to indicate peak current asymmetry. We consider several forms of

633 skewness measure and conclude that a filtered derivative skewness has better
634 explanatory power. The skewness measure is applicable for all tidal environments and
635 in particular for mixed tidal regimes. The skewness measure is able to reveal subtidal
636 variations of tidal asymmetry and the relative contribution of different tidal
637 interactions under mixed regimes. The harmonic and statistical skewness methods are
638 not mutually exclusive but can be qualitatively linked.

639 Using the skewness measure, we find that the M_2 - M_4 interaction induces much
640 stronger tidal asymmetry even with small M_4 amplitude compared to other tidal
641 interactions. We confirm that tidal asymmetry is stronger during spring tide than neap
642 tide and it exhibits distinctive behaviors in response to low and high river discharges
643 between the upper and lower regions of long estuaries. We see that slack water
644 asymmetry is relatively poorly studied compared to peak current asymmetry and more
645 work is needed regarding its controlling effect on residual fine sediment transport.

646

647

648 **Acknowledgements**

649 This work is supported by the project 'Coping with deltas in transition' within the
650 Programme of Strategic Scientific Alliance between China and The Netherlands
651 (PSA), financed by the Ministry of Science and Technology, P.R. China (MOST) (No.
652 2016YFE0133700) and Royal Netherlands Academy of Arts and Sciences (KNAW)
653 (No. PSA-SA-E-02), and also by National Natural Science Foundation of China (Nos.
654 51320105005, 51739005, 41506105, 41876091), and Shanghai Committee of Science
655 and Technology (Nos. 17DZ1204800, 16DZ1205403). L. Guo is also funded by
656 SKLEC-Fund (No. 2015RCDW02). We thank the two anonymous reviewers for their
657 constructive comments.

658

659

660 **References**

661 Aubrey D.G., Speer P.E., 1985. A study of non-linear tidal propagation in shallow
662 inlet/estuarine systems. Part I: Observations. Estuarine, Coastal and Shelf Science

663 21, 185-205.

664 Blanton J.O., Lin G., Elston S.A., 2002. Tidal current asymmetry in shallow estuaries
665 and tidal creeks. *Continental Shelf Research* 22, 1731-1743.

666 Bruder B., Bomminayuni S., Hass K., Stoesser T., 2014. Modeling tidal distortion in
667 the Ogeechee Estuary. *Ocean Modeling* 82, 60-69.

668 Cai H.Y., Savenije H.H.G., Jiang C.J., Zhao L.L., Yang Q.S., 2016. Analytical
669 approach for determining the mean water level profile in an estuary with substantial
670 freshwater discharge. *Hydrology Earth System Science* 20, 1177-1195.

671 Castanedo S., Mendez F.J., Medina R., Abascal A.J., 2007. Long-term tidal level
672 distribution using a wave-by-wave approach. *Advances in Water Resources* 30,
673 2271-282.

674 de Swart H.E., Zimmerman J.T.F., 2009. Morphodynamics of tidal inlet systems.
675 *Annual Review of Fluid Mechanics* 41, 203–229.

676 Dronkers J., 1986. Tidal asymmetry and estuarine morphology. *Netherlands Journal of*
677 *Sea Research* 20(2/3), 107-131.

678 Friedrichs C.T., Aubrey D.G., 1988. Non-linear tidal distortion in shallow well-mixed
679 estuaries: a synthesis. *Estuarine, Coastal and Shelf Science* 27, 521-545.

680 Gallo M.N., Vinzon S.B., 2005. Generation of overtides and compound tides in the
681 Amazon Estuary. *Ocean Dynamics* 55, 441-448.

682 Gatto V.M., van Prooijen B.C., Wang Z.B., 2017. Net sediment transport in tidal
683 basins: quantifying the tidal barotropic mechanisms in a unified framework. *Ocean*
684 *Dynamics*, doi:10.1007/s10236-017-1099-3.

685 Godin G., 1985. Modification of river tides by the discharge. *Journal of Waterway,*
686 *Port, Coastal and Ocean Engineering* 111(2), 257–274.

687 Godin G., 1991. Frictional effects in river tides. In: B.B. Parker (ed.), *Tidal*
688 *hydrodynamics*, John Wiley, Toronto, pp.379–402.

689 Gong W.P., Schuttelaars H., Zhang H., 2016. Tidal asymmetry in a funnel-shaped
690 estuary with mixed semidiurnal tides. *Ocean Dynamics* 66, 637-658.

691 Guo L.C., van der Wegen M., Roelvink J.A., He Q., 2014. The role of river flow and
692 tidal asymmetry on 1D estuarine morphodynamics. *Journal of Geophysical*

693 Research: Earth Surface 119, doi: 10.1002/2014JF003110.

694 Guo L.C., van der Wegen M., Jay D.A., Matte P., Wang Z.B., Roelvink J.A., He Q.,
695 2015. River-tide dynamics: exploration of nonstationary and nonlinear tidal
696 behavior in the Yangtze River estuary. *Journal of Geophysical Research: Oceans*
697 120, doi:10.1002/2014JC010491.

698 Guo L.C., van der Wegen M., Wang Z.B., Roelvink J.A., He Q., 2016a. Exploring the
699 impacts of multiple tidal constituents and varying river flow on long-term, large
700 scale estuarine morphodynamics by means of a 1D model. *Journal of Geophysical*
701 *Research: Earth Surface* 120, doi:10.1002/2016JF003821.

702 Guo L.C., Brand M., Sanders B.F., Foufoula-Georgiou E., Stein E., 2018. Tidal
703 asymmetry and its variability in a short tidal basin with implications on residual
704 sediment transport and basin management. moderately revised in *Advances in Water*
705 *Resources*.

706 Guo W.Y., Song D.H., Wang X.H., Ding P.X., Ge J.Z., 2016b. Contributions of
707 different tidal interactions to fortnightly variations in tidal duration asymmetry.
708 *Journal of Geophysical Research: Oceans* 121, 5980-5994.

709 Hoitink A.J.F., Hoekstra P., van Maren D.S., 2003. Flow asymmetry associated with
710 astronomical tides: implications for the residual transport of sediment. *Journal of*
711 *Geophysical Research* 108(C10), 3315–3322.

712 Jay D.A., Leffler K., Diefenderfer H.L., Borde A.B., 2014. Tidal-fluvial and estuarine
713 processes in the lower Columbia River: I. along-channel water level variations,
714 Pacific Ocean to Bonneville Dam. *Estuaries and Coasts*, doi:
715 10.1007/s12237-014-9819-0.

716 Jewell S.A., Walker D.J., Fortunato A.B., 2012. Tidal asymmetry in a coastal lagoon
717 subject to a mixed tidal regime. *Geomorphology* 138, 171-180.

718 Le Provost C., 1991. Generation of overtides and compound tides (review). In: B.B.
719 Parker (ed.), *Tidal Hydrodynamics*, John Wiley, Toronto, pp.269–295.

720 LeBlond P.H., 1991. Tides and their interactions with other oceanographic phenomena
721 in shallow water (review). In: B.B. Parker (ed.), *Tidal Hydrodynamics*, John Willey,
722 Toronto, pp. 357-378.

723 Levoy F., Anthony E.J., Dronkers J, Monfort O., Izabel G., Larssonneur C., 2017.
724 Influence of the 18.6-year lunar nodal tidal cycle on tidal flats: Mont-Saint-Michel
725 Bay, France. *Marine Geology* 387, 108-113.

726 Lincoln J.M., Fitzgerald D.M., 1988. Tidal distortion and flood dominance at five
727 small tidal inlets in southern Maine. *Marine Geology* 82, 133-148.

728 Matte P., Jay D.A., Zaron E.D., 2013. Adaptation of classical tidal harmonic analysis
729 to nonstationary tides, with application to river tides. *Journal of Atmospheric and*
730 *Oceanic Technology* 30(3), 569–589.

731 Nidzieko N.J., 2010. Tidal asymmetry in estuaries with mixed semidiurnal/diurnal
732 tides. *Journal of Geophysical Research* 115, C08006, doi:10.1029/2009JC005864.

733 Pawlowicz R., Beardsley, B., Lentz, S., 2002. Classical tidal harmonic analysis
734 including error estimates in MATLAB using T_TIDE. *Computers & Geosciences* 28,
735 929–937.

736 Postma H., 1961. Transport and accumulation of suspended matter in the Dutch
737 Wadden Sea. *Netherlands Journal of Sea Research* 1, 148–190.

738 Ranasinghe R., Pattiaratchi C., 2000. Tidal inlet velocity asymmetry in diurnal
739 regimes. *Continental Shelf Research* 20, 2347–2366.

740 Ruessink B.G., van den Berg T.J.J., van Rijn L.C., 2009. Modeling sediment transport
741 beneath skewed asymmetric wave above a plane bed. *Journal of Geophysical*
742 *Research* 114, C11021, doi:10.1029/2009JC005416.

743 Reichman B.O., Muhlestein M.B., Gee K.L., Neilson T.B., Thomas D.C., 2016.
744 Evolution of the derivative skewness for nonlinearly propagating waves. *The*
745 *Journal of the Acoustical Society of America* 139, 1390-1403.

746 Sassi M.G., Hoitink A.J.F., 2013. River flow controls on tides and tide-mean water
747 level profiles in a tidal freshwater river. *Journal of Geophysical Research: Ocean*
748 118, doi:10.1002/jgrc.20297.

749 Shepherd M.R., Gee K.L., Hanford A.D., 2011. Evolution of statistical properties for a
750 nonlinearly propagating sinusoid. *The Journal of the Acoustical Society of America*
751 130, EL8-13.

752 Song D.H., Wang X.H., Kiss A.E., Bao X.W., 2011. The contribution of tidal

753 asymmetry by different combinations of tidal constituents. *Journal of Geophysical*
754 *Research* 116, C12007, doi:10.1029/2011JC007270.

755 Speer P.E., Aubrey D.G., 1985. A study of non-linear tidal propagation in shallow
756 inlet/estuarine systems. Part II: Theory. *Estuarine, Coastal and Shelf Science* 21,
757 207-224.

758 Speer P.E., Aubrey D.G., Friedrichs C.T., 1991. Non linear hydrodynamics of shallow
759 tidal inlet/bay systems. In: B.B. Parker (ed.), *Tidal Hydrodynamics*, John Wiley,
760 Toronto, pp.321–339.

761 Toubanc F., Brenon I., Coulombier I., Le Moine O., 2015. Fortnightly tidal
762 asymmetry inversions and perspectives on sediment dynamics in a macrotidal
763 estuary (Charente, France). *Continental Shelf Research* 94, 42-54.

764 van de Kreeke J., Robaczewska K., 1993. Tide-induced residual transport of coarse
765 sediment: application to the Ems Estuary. *Netherlands Journal of Sea Research*
766 31(3), 209–220.

767 van Rijn L.C., 1993. *Principles of sediment transport in rivers, estuaries and coastal*
768 *seas*. Aqua Publications, the Netherlands.

769 Wang Z.B., Juken H., de Vriend H.J., 1999. Tidal asymmetry and residual sediment
770 transport in estuaries. WL|Hydraulic, report No. Z2749, 66 pp.

771 Wang Z.B., Jeuken C., Gerritsen H., de Vriend H.J., Kornman B.A., 2002.
772 Morphology and asymmetry of the vertical tide in the Westerschelde estuary.
773 *Continental Shelf Research* 22, 2599–2609.

774 Wang Z.B., Townend I., 2012. Influence of the nodal tide on the morphological
775 response of estuaries. *Marine Geology* 291-294, 73-82.

776 Zhang M, Townend I, Zhou Y.X., Cai H.Y., 2016. Seasonal variation of river and tide
777 energy in the Yangtze estuary, China. *Earth Surface Processes and Landforms* 41,
778 98-116.

779 Zhou Z., Coco G., Townend I., Gong Z., Wang Z.B., Zhang C.K., 2018. On the
780 stability relationships between tidal asymmetry and morphologies of tidal basins and
781 estuaries. *Earth Surface Processes and Landforms*, doi:10.1002/esp.4366.

782

783 **Captions of Table and Figures**

784

785 **Table 1.** Summary of the methods available for quantification of tidal asymmetry. θ
786 and Φ indicate the phase of vertical and horizontal tidal components, respectively. A
787 and U are amplitudes of vertical and horizontal tides, respectively.

788 **Figure 1.** Sketch of the Changjiang River estuary and tidal gauges. The numbers in
789 the brackets indicate the seaward distance to Datong, the tidal wave limit in the dry
790 season. Niupijiao represents the river mouth, and Xuliujing and Nanjing represents
791 the lower and upper estuary, respectively, with the division roughly at Jiangyin (Guo
792 et al., 2015). QLG is the abbreviation of Qinglonggang. The smaller dots indicate
793 other tidal gauges though their data are not included in this work.

794 **Figure 2.** Tidal heights by M_2 , M_4 and M_2+M_4 tides with a phase difference $2\theta_{M_2}-\theta_{M_4}$
795 of (a) 0° , (b) 90° , (c) 180° , and (d) 270° . The A_{M_4}/A_{M_2} amplitude ratio is 0.3.

796 **Figure 3.** (a) Skewed and (b) asymmetric tidal wave or tidal current curves, and (c, d)
797 their corresponding PDFs. The positively and negatively asymmetric curves in pane
798 (b) have the same PDF thus they are overlapped in panel (d). The flood currents are
799 positive and ebb currents are negative in panel (a) and (b).

800 **Figure 4.** The PDFs of tidal heights (a, b, c) and tidal durations (d, e, f) at stations in
801 the upper estuary (landward regions, Nanjing in Figure 1) (a, d), lower estuary
802 (seaward regions, Xuliujing) (b, e) and estuary mouth (Niupijiao) (c, f) based on
803 2-year data (2009-2010) in the Changjiang River estuary. The tidal heights are
804 referenced to local mean water level. Rising tidal duration is positive and falling
805 tidal duration is negative.

806 **Figure 5.** (a) River discharge in calendar year 2010, (b) high-passed filtered tidal
807 height, tidal ranges, and filtered derivative skewness in the (b) upper estuary
808 (Nanjing, see Figure 1) and (c) lower estuary (Xuliujing), and (d) derivative
809 skewness vs. tidal range, and (e) derivative skewness vs. river discharge in the
810 Changjiang River estuary.

811 **Figure 6.** Scatter plot of filtered derivative skewness of tidal duration asymmetry due
812 to (a) M_2 - M_4 and (b) M_2 - O_1 - K_1 interactions for ideally constructed signals with

813 different phase differences and amplitude ratios, and (c, d) variations of derivative
814 skewness and transformed skewness for an amplitude ratio of 0.3 but different phase
815 differences. Positive derivative skewness and negative transformed skewness
816 suggest flood dominance.